International Journal of Nanoelectronics and Materials
IJNeaM
ISSN 198-5761 | E-ISSN 2232-1535

Fabrication and Characterization of Eco-Friendly Screen-Printed Electrode Using Activated Rice Husk Carbon Ink for Electrochemical Detection of SAR-CoV-2

Athirah Amir[a], Shahidah Arina Shamsuddin[a,b,*], Adilah Ayoib[a,c], Subash Gopinath[a,c], Muhammad Ikman Ishak[b], Mohd Nazree Derman[b], Muhammad Kashif[d]

[a]*Institute of Nano Electronic Engineering, Universiti Malaysia Perlis (UniMAP), Seriab, 01000 Kangar, Perlis, Malaysia*
[b]*Faculty of Mechanical Engineering & Technology, Universiti Malaysia Perlis (UniMAP), 02600, Arau, Perlis, Malaysia*
[c]*Faculty of Chemical Engineering & Technology, Universiti Malaysia Perlis (UniMAP), 02100, Padang Besar, Perlis, Malaysia*
[d]*School of Electrical and Information engineering, Tianjin University, 300072, Tianjin, China*
**Corresponding author. Tel.: +011-11254595; e-mail: shahidaharina@unimap.edu.my*

Received 22 Jul 2025, Revised 7 May 2026, Accepted 21 May 2026

ABSTRACT

Rice husk in Malaysia has been treated as agricultural waste until now. It is usually burnt for disposal, which has caused air pollution. Few researchers have sought to reduce this pollution by transforming rice husk into useful products, such as composite panels for furniture. Similar to other organic substances, rice husk can be treated to become activated carbon through a controlled carbonization and activation process. Activated rice husk carbon has been reported to be developed for multiple uses, such as in battery storage or fertilizer applications, due to its high porosity properties and its flexibility to be surface-modified with various functional groups. This study focuses on developing a conductive ink based on activated rice husk carbon (ARHC) to enhance the performance of conventional screen-printed electrodes (SPEs) for detecting SARS-CoV-2 (COVID-19). To synthesize the ARHC, rice husk was carbonized at 500°C for 2 hours and further treated with an activation process at 850°C for 2 hours in NaOH soaking. To prepare the conductive ink, the synthesized ARHC was mixed with chitosan. The ARHC conductive ink was then applied on the conventional SPE's working electrode (WE) surface. The synthesized ARHC was characterized through surface morphology (SEM and FESEM), surface area (BET), surface functionality (FTIR and EDX), and crystallinity (XRD). For the COVID-19 detection test, the ARHC WE were first functionalized with (3-Aminopropyl) triethoxysilane (APTES) and further immobilized with spike protein (SP) antibodies. These surface modification steps enable selective detection of SARS-CoV-2 through the spike protein (SP) target. For sensitivity analysis, a current-voltage (I-V) test was carried out across various concentrations of SP targets, ranging from micromolar to picomolar. All these results were compared with those of the original conventional carbon SPE to determine whether implementing ARHC in the SPE system could enhance the performance of SPE as a COVID-19 biosensor. Based on the project findings, hydroxyl (OH) groups formed on the ARHC surface after synthesis enhance its sensitivity and selectivity toward specific biomolecules, making it a promising candidate for the development of low-cost and eco-friendly biosensors. The ARHC-SPE provides a real-time, label-free platform for detecting COVID-19 and uses agricultural waste as an efficient early-detection tool that helps prevent the further spread of infectious diseases.

Keywords: *Activated rice husk carbon, Agricultural waste valorization, Circular economy, Biosensor technology, Screen-printed electrode, SARS-CoV-2 spike protein detection*

1. INTRODUCTION

The worldwide need to contain the transmission of COVID-19 underscores the critical requirement for rapid, user-friendly, and highly sensitive testing techniques. Existing conventional diagnostic methods, such as RT-PCR, are sensitive and expensive and highly dependent on sophisticated laboratory infrastructure, making them unsuitable for point-of-care testing [1, 2]. The technique is also labour intensive and invariably requires highly trained professionals to analyze the results and skilled personnel to obtain nasopharyngeal swabs [3]. Furthermore, the entire test process usually takes around three to four hours, making it highly unsuitable for rapid diagnoses. This has prompted extensive research to develop portable, reasonably priced biosensors that provide instant results across various applications [3-5]. The presently available test kits that come into the market are mainly based on the qualitative lateral flow assay (LFA) technique, which relies on visual interpretation and calls for comparatively large samples and, sometimes complicated preparation to isolate the sample. These requirements increase the likelihood of false outcomes [6]. In contrast, biosensor-based tests that use electrochemical detection enable simultaneous detection of COVID-19 and generate quantitative, real-time, truthful, label-free results from only a small amount of saliva.

This advanced design removes the tedious process of protein extraction and the subjective visual qualitative index by giving numerical output. The electrochemical biosensor, one of the promising detection platforms for viral biomarkers because of its high detection sensitivity, simplicity, user-friendliness, and compatibility with mass production, has been improved [1, 3, 4, 7-9]. The performance of the electrodes fully depends on the nature

of the advanced material used as the working electrode [4]. The working electrode surface is optimized through surface modification by introducing more functional groups to the surface [1,4]. With so many choices of advanced materials, such as carbon nanotube, nanodiamond, gold nanoparticle, silver nanoparticle, silicon nanowire, activated carbon, etc., Activated Rice Husk Carbon (ARHC), which is derived from rice husk waste material through controlled carbonization followed by an activation process, would be a more inexpensive and environmentally friendly advanced material for electrode improvement [10-12].

The parameters used during the synthesis and activation process (carbonization temperature and activation temperature) will definitely affect the pore structure and the surface chemistry of the activated rice husk carbon (ARHC) [13, 14]. Carbonization at a temperature of 500°C will ensure that the organic compounds decompose, while an additional activation process at a temperature of 850°C with the addition of NaOH as the activator can form a good conductive activated rice husk carbon (ARHC) [11,14]. This work investigates the effect of important synthesis parameters, carbonisation at 500 °C and activation at 850 °C, on the electrochemical response of ARHC as a biosensing material within SPEs for the detection of COVID-19. The influence of these conditions on surface groups, surface area, porosity, conductivity, and sensitivity is discussed. These impacts are vital for the design of rapid, sustainable, and reliable biosensors [4, 7, 8]. The study also aims to demonstrate that ARHC, when used as a recycled waste material transformed into a value-added product, can significantly enhance SPE performance, particularly by improving detection sensitivity. The findings are expected to open new research opportunities and support further optimization of ARHC's synthesis and performance.

2. MATERIAL AND METHODS

2.1 Material and Chemicals

The primary material used in this study was rice husk sourced from Dibuk Sdn. Bhd, Kedah (HQ). Chemical activation was carried out using a sodium hydroxide (NaOH) solution (Sigma-Aldrich) at 10 wt% concentration. 2 w/v% chitosan in acetic acid (Sigma-Aldrich) was used as the binder to prepare the ARHC conductive ink. A 2% (v/v) solution of 3-aminopropyl triethoxysilane, APTES (Sigma-Aldrich) in ethanol, PBASE (Sigma-Aldrich), spike protein (SP) antibodies (Bita Lifescience Sdn. Bhd.) and spike protein (SP) (Bita Lifescience Sdn. Bhd.) were used for ARHC surface modification, as well as the immobilization and hybridization processes. Meanwhile, deionized water and phosphate-buffered saline, or PBS (Sigma-Aldrich) were used for solution preparation and regular rinsing, respectively.

2.2 Preparation of Carbonized Rice Husk (CRH), Activated Rice Husk Carbon (ARHC) and Conductive ARHC Ink

The rice husk was subjected to carbonization in a programmable tube furnace under a continuous nitrogen gas flow to create an inert atmosphere. The temperature was ramped from room temperature to 500 °C at a rate of 10 °C/min and maintained at 500 °C for 2 hours to ensure complete carbonization. After 2 hours, the carbonized rice husk was allowed to cool to room temperature. Next, the carbonized rice husk was chemically activated at high temperature while soaked in sodium hydroxide, at 850 °C with a heating rate of 10 °C/min and maintained for 2 hours under a nitrogen atmosphere. The resulting ARHC was allowed to cool to room temperature. After cooling to room temperature, the resulting ARHC was rinsed with deionized water until a neutral pH (~7.0) was reached and dried in a vacuum oven for 24 hours to remove moisture. To prepare the ARHC conductive ink, ARHC powder was mixed with 2 w/v% of chitosan in acetic acid. 10 µL of the composite mixture wasappliped to the SPE working electrode and allowed to dry at room temperature.

2.3 Material Characterisation of Raw, Carbonized Rice Husk (CRH) and Activated Rice Husk Carbon (ARHC)

For characterization, scanning electron microscopy (SEM) was used to examine morphological changes and the development of porosity before and after the activation treatment. In addition, SEM was used to observe the surface morphology of the ARHC–chitosan mixture on the SPE working electrode's surface. Fourier-transform infrared (FTIR) spectroscopy was used to analyze surface functional groups, recording spectra in the range of 4000–400 cm^{-1} with a resolution of 4 cm^{-1} and 32 scans per sample. X-ray diffraction (XRD) analysis provided insight into changes in the samples' crystallinity. Brunauer–Emmett–Teller (BET) surface area, pore size distribution, and porosity were measured via nitrogen adsorption-desorption isotherms. BET calculations provided specific surface areas for raw rice husk, CRH and ARHC.

2.4 ARHC Surface Modification, Immobilization and Hybridization

For surface modification, 10 µL of 2% (v/v) APTES in ethanol solution was applied on the ARHC surface and incubated for 60 minutes. After 60 minutes, the electrode was rinsed with 0.1 M PBS solution to remove any excess unbound silane. Next, 10 µL of pyrene-based succinimide ester (PBASE) was applied to enhance interactions with the hydroxyl-rich ARHC surface, supporting stable attachment of bio-recognition elements. The surface was incubated for 60 minutes. To immobilize biorecognition elements, 10 µL of 10 µM spike protein (SP) antibodies was dropped onto the ARHC/APTES/PBASE and incubated for 60 minutes. Following incubation, unbound antibodies were removed by rinsing the electrodes with PBS to ensure effective immobilization while preserving the structural and electrochemical integrity of the ARHC-SPE surface. 1%

(w/v) polyethylene glycol (PEG) in PBS was then used as a blocking agent prior to electrochemical testing to reduce nonspecific adsorption. During the hybridization process, 10 µL of spike protein (SP) targets was applied onto the ARHC/APTES/PBASE/PEG/anti-SP and incubated for 5 minutes. The unbound targets were then removed by rinsing with PBS solution. The immunogens performance (hybridization test) of the ARHC-modified electrodes was then evaluated through the specific interactions between immobilized SP antibodies and SP proteins, as shown by the current response in the current-voltage test (I-V).

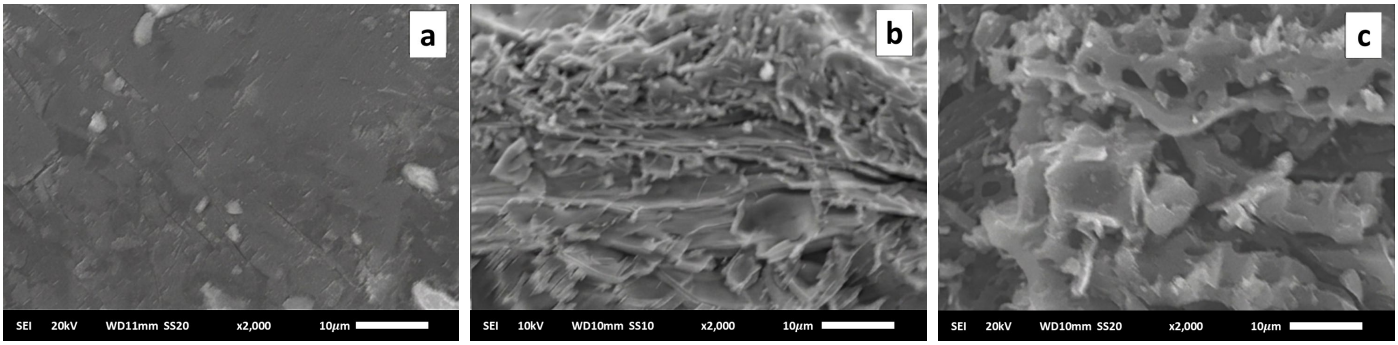

Figure 1. SEM images illustrating the surface morphological structure of raw rice husk (a), CRH (b), and ARHC (c).

2.5 Sensitivity Measurement

Current–voltage testing (I–V test) was conducted to measure and evaluate the sensitivity performance of ARHC-modified SPE for detecting the COVID-19 (SP) target across seven different concentrations: 1 fM, 10 fM, 100 fM, 1 pM, 10 pM, 100 pM and 1 nM.

Following hybridization with the target, 5 µL of redox solution containing 5 mM ferri/ferrocyanide in 1.0 M KCl ($[Fe(CN)_6]^{3-}/[Fe(CN)_6]^{4-}$) was dropped onto the SPE electrode surface before the measurement. The I-V test was performed using the Autolab PGSTAT, with the applied voltage ranging from 0 V to 1.0 V. After measurement, the SPE was rinsed with PBS and dried with a hand blower before proceeding to the next concentration. The test was conducted sequentially from the lowest to the highest target concentration, with the same procedure repeated for each concentration.

3. RESULTS AND DISCUSSION

3.1 Morphological Characterization

The morphological evolution of the rice husk across different thermochemical treatment stages, as depicted in Scanning Electron Microscopy (SEM) images, reveals a systematic development of porosity essential for electrochemical applications [10,11,14]. Figure 1 shows the initial raw rice husk (Figure 1a) presents a relatively dense, non-porous, and smooth surface morphology. Following carbonization at 500°C (Figure 1b), the structure undergoes a noticeable transformation, where the removal of volatile organic matter results in the formation of a more granular and roughened surface, indicating the initial development of a porous carbon matrix. The most significant change occurs after NaOH activation at high-temperature (Figure 1c), which creates a highly developed, sponge-like structure with a network of interconnected macropores and mesopores. At higher temperatures above 500°C, NaOH acts as an oxidizing and etching agent that penetrates the carbon structure, removing impurities, as well as amorphous carbon by breaking up the C-C, C-O-C bonds, generating active sites by introducing oxygen-containing functional groups such as C-O, C=O, C-OH, and -COONa. At the same time, CO, CO_2, and H_2 gases are produced as by-products from the reactions between NaOH and carbon. These gases contribute to the formation of micro- and mesopores within the carbon matrix [15]. Meanwhile, the formation of carbonates and alkali metals (Na) within the carbon matrix contributes to the stabilization and expansion of the interlayer spacing between carbon atoms. Therefore, increasing the sodium hydroxide ratio during the activation process enhances pore development, resulting in a larger surface area and greater pore volume. During the water-rinsing stage until pH 7.0, sodium carboxylate groups (-COONa) are protonated into carboxylic acid groups (COOH), producing a highly porous activated carbon surface enriched with oxygen-containing functional groups.

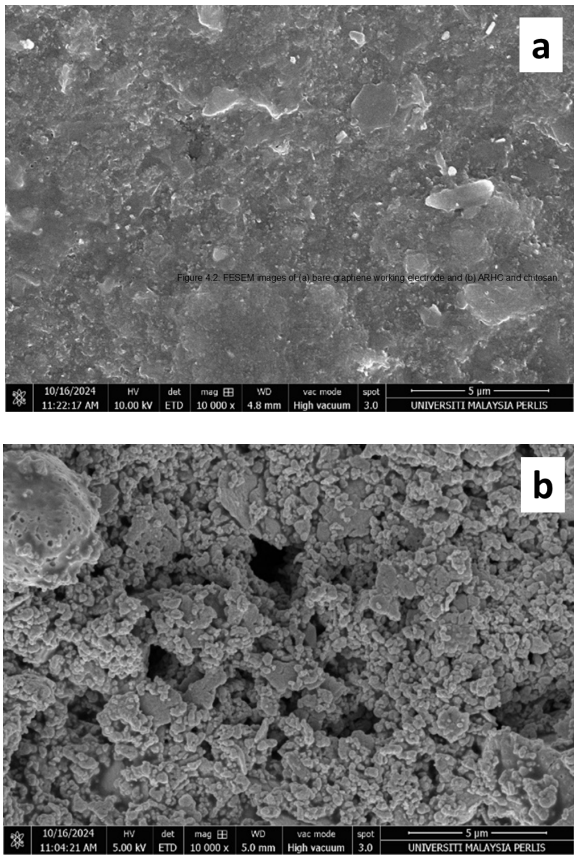

Figure 2. FESEM images of SPE's working electrode surfaces with (a) bare graphite and (b) ARHC-chitosan.

In the next stage, ARHC is mixed with the chitosan solution to ensure adhesion on the SPE working electrode surfaces while ensuring that conductivity is not reduced. Figure 2a shows the bare SPE, which has a relatively flat, granular surface characteristic of the underlying conventional graphite carbon ink, which offers a limited electroactive surface area. In contrast, Figure 2b shows that the ARHC-chitosan SPE has a highly porous, three-dimensional, and rougher topography [10,11,14]. The ARHC surfaces were uniformly covered by the chitosan. This porous morphology is crucial for biosensing applications, as it significantly increases the electrode's specific surface area. The enlarged surface area and well-developed, interconnected porous network of ARHC enhance loading capacity, improve mass transport of the target analyte to the electrode surface, and accelerate electron-transfer kinetics [16]. This augmented surface provides a higher density of active sites for effective immobilization of biorecognition probes (anti-SARS-CoV-2 spike protein antibodies) [3,5,7,8]. The combined effects amplify the electrochemical signal, resulting in improved sensitivity and a lower limit of detection. The rice husk-derived activated carbon is a promising, low-cost nanomaterial for fabricating sensitive, disposable SPE-based electrochemical biosensors for point-of-care COVID-19 diagnostics.

3.2 Crystallinity Analysis

The X-ray diffraction (XRD) patterns confirm the shift from the ordered structure between raw rice husk and highly amorphous activated carbon. As shown in Figure 3 (black line), the raw rice husk diffraction pattern exhibited a broad diffuse feature at about $2\theta = 22$ °, which is characteristic of amorphous silica and semi-crystalline structures in cellulosic materials within the biomass. The intensity of such a peak was greatly suppressed and broadened after char formation at 500°C (red line), which could be attributed to the evolution of crystalline cellulose into an amorphous carbon structure, such as carbonaceous material. The final product ARHC (green line) pattern demonstrated two broad diffraction maxima at about $2\theta = 24$ and 43, corresponding to the (002) and (100) turbostratic planes of the amorphous carbon, respectively [10, 11, 14].

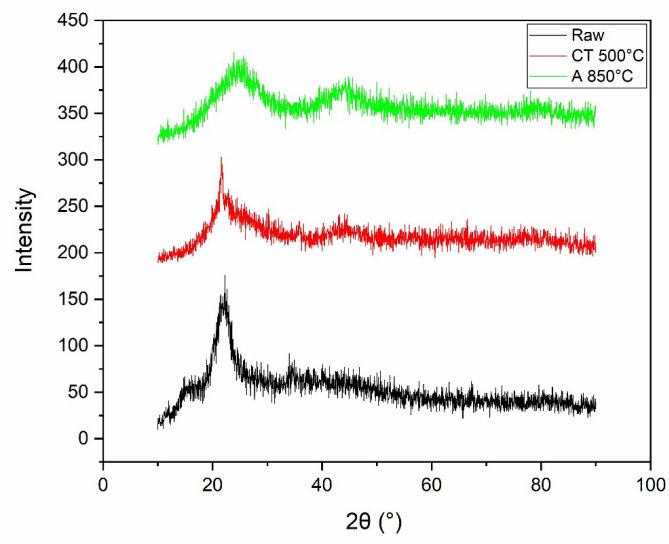

Figure 3. XRD pattern of raw rice husk, CRH and ARHC.

The porous structure of this activated carbon is highly beneficial for biosensor applications, particularly as a sensing material in the working electrode of screen-printed electrodes (SPEs) for detecting SARS-CoV-2. Due to the high surface area, the activated carbon offers more surface for biomolecules like the RNA or proteins of the virus, to be adsorbed and enriched from biological matrices comprising many potentially interfering molecules (saliva/nasal swabs). In addition, the carbon surface chemistry allows the material to physically capture the analyte through hydrophobic forces and π–π stacking interactions. This high surface area structure of the activated carbon, due to its amorphous structure, can greatly increase the sensitivity and dependability of subsequent biosensor detection of the virus.

3.3 Surface Functionalities Analysis

The Fourier-transform infrared (FTIR) spectroscopy results effectively map the chemical transformation of the rice husk at each processing stage. Figure 4 shows the FTIR spectra of raw, CRH and ARHC. A broad absorption band centered around 3350 cm^{-1} is observed in all samples and is attributed to O–H stretching vibrations from surface hydroxyl groups and adsorbed moisture. Peaks of aliphatic C–H stretching near 2900 cm^{-1} were observed in all samples, which represent cellulose and hemicellulose from the raw rice husk's original substance. However, the peaks were reduced and disappeared after carbonization and activation, indicating the successful thermal decomposition of the primary organic components. At the same time, a very strong and broad peak centered at approximately 1080 cm^{-1} along with a sharp peak at ~800 cm^{-1}, IS assigned to the classic asymmetric and symmetric stretching vibrations of Si-O-Si bonds in silica (SiO_2). The significant reduction in all organic functional groups and the emergence of these prominent silica bands confirm the formation of a carbon-silica composite material with a silica-rich surface [10,11,14].

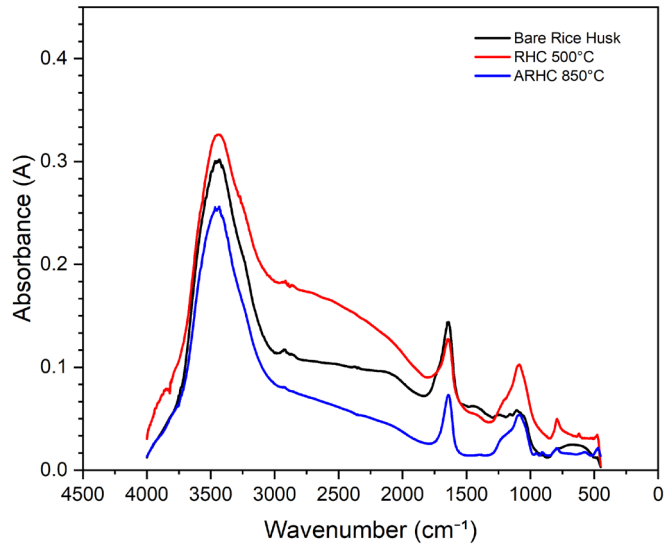

Figure 4. FTIR absorbance spectra of raw rice husk, CRH and ARHC.

The concurrent increase of all peaks at 3350 cm^{-1} (O-H stretching vibrations from surface hydroxyl groups), 1637 cm^{-1}(C=C stretching vibrations of aromatic carbon structures) and 1085 cm^{-1} (C–O stretching vibrations) of all samples confirms the formation of oxygenated moieties, particularly carboxylic groups (-COOH), in ARHC derived from raw rice husk. In the COVID-19 biosensor application, the carboxylic groups present on ARHC can be effectively functionalized with APTES to establish a strong amide linkage. APTES contains two terminal $-NH_2$ groups located at both ends of its molecular structure. During functionalization, one of the $-NH_2$ groups binds to the carboxyl groups on ARHC surfaces, while the other $-NH_2$ group reacts with the -COOH of SP antibodies during the immobilization of biorecognition elements. Hence, the presence of carboxylic groups on ARHC is essential for efficient biosensor performance. A higher density of this group generally improves the biosensor sensitivity and overall performance.

3.4 Porosity and Surface Area Analysis

The nitrogen adsorption–desorption isotherms of the raw rice husk, CRH, and ARHC are presented in Figure 5. The raw rice husk exhibits a typical Type II isotherm according to the IUPAC classification, which is characteristic of nonporous or macroporous materials. This behavior is evidenced by the very low nitrogen uptake at low relative pressures ($P/P_0 <$ 0.1) and the gradual increase in adsorbed volume at higher relative pressures, indicating the predominance of external surface adsorption with minimal micro- or mesoporosity. However, the isotherm for the CRH displays Type IV with an H_4-type hysteresis loop, indicative of the formation of mesopores with slit-shaped pores seen in carbons. The initial rapid uptake at low P/P_0 corresponds to the filling of micropores, the hysteresis at 0.4–0.9 P/P_0 is due to capillary condensation of the adsorbate in mesopores. When activated at 850°C, the ARHC sample shows a composite isotherm combining type I and type IV adsorption with an H_4 hysteresis loop, which implies abundant micropore and mesopore formations [11,14], and agrees well with the overall higher adsorption amount along the whole of the P/P_0 adaptation range. The very sharp nitrogen adsorption at very low P/P_0 range is an indication of micropore domination, and the H_4 hysteresis points to the presence of mesopores. These data overall clearly reflect the nonporous nature of the raw rice husks through to the mesoporous structure after carbonization, and on to the micro mesoporous activated carbon with a considerable rise in surface area and pore volume.

Table 1 also shows the nitrogen adsorption–desorption data. There are clear changes in the surface characteristics of the rice husk after carbonization and chemical activation. The apparent surface area of the raw rice husk was very small (3.55 $m^2\ g^{-1}$) with total pore volume of (0.0107 $cm^3\ g^{-1}$) and no visible microporosity (pore diameter of 48.7 nm). This is expected given the limited porous structure of the material. Carbonization at 500 °C improved the surface architecture of the rice husk, with a surface area of 246.2 m^2/g and pore volume of 0.1225 cm^3/g, while releasing a significant amount of pre-existing volatile compounds as evident by the micropore surface area of 220.0 m^2/g, micropore volume of 0.111 cm^3/g, and average pore diameter of 2.58 nm. The chemical activation at 850 °C in combination with NaOH caused a similar increase in surface area to 243.6 $m^2\ g^{-1}$, but almost doubled the total pore volume to 0.281 $cm^3\ g^{-1}$, with the pore diameter increasing to 4.61 nm. It is interesting to observe that, despite a reduction in micropore surface area to 161.5 m^2/g, the shift toward larger mesopores indicates that activation both generates new pore channels and alters the structure toward a more accessible porous network. The excess mesoporous surface could be beneficial for electrochemical biosensing, as it enables faster diffusion of electrolyte ions and biomolecules while maintaining a high surface area for effective analyte adsorption. So, from the raw rice husk through to the CRH and final ARHC, the combined benefit of the thermal treatment and alkaline activation is highlighted by the effects on surface area, pore volume, and pore size distribution.

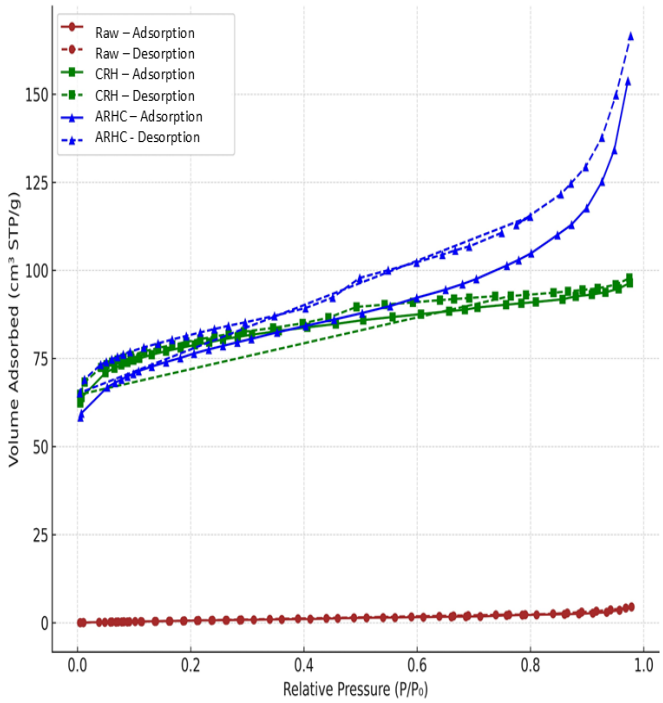

Figure 5. Nitrogen Adsorption-Desorption Isotherms of raw rice husk, CRH and ARHC.

Table 1 BET surface area, pore volume and Isotherm TYPE, carbonized (CT500), and activated (A850) rice husk carbon

Sample	BET SA (m^2/g)	Pore Volume (cm^3/g)	Average Pore Diameter (Å)	Micropore SA (m^2/g)	Micropore Vol (cm^3/g)	Isotherm Type/ Hysteresis
Raw Rice Husk	3.55	0.0107	6.03	0.00	0.00	Type II (nonporous/macroporous)
Rice Husk Carbonized at 500°C	246.2	0.159	2.58	220.0	0.111	Type IV-H4 (mesoporous)
Rice Husk Activated at 850°C	243.6	0.281	4.61	161.5	0.081	Type I/IV-H4 (micro–mesoporous)

3.5 I-V Measurement and Sensitivity Analysis

I–V measurement tests using a PGSTAT were conducted to study the performance comparison between bare SPE and ARHC-SPE in detecting COVID-19. Figure 6 shows the I-V curve of the bare SPE after being modified with APTES/antibody/PEG, while detecting the COVID-19 target analyte at varying concentrations, including a real saliva sample (non-infected). The readings start with the bare SPE electrode, APTES modification, and SP antibody immobilization process, followed by PEG (polyethylene glycol) as the blocking agent. Once the bare SPE was immobilized and ready for use, various testing samples including deionized water, PBS (phosphate-buffered saline), saliva samples 1 and 2 (for non-infected control), and SP target at varying concentrations ranging from 1 fM to 1 nM were tested to assess the sensitivity and selectivity of the ARHC-SPE in detecting the specific SP target analyte.

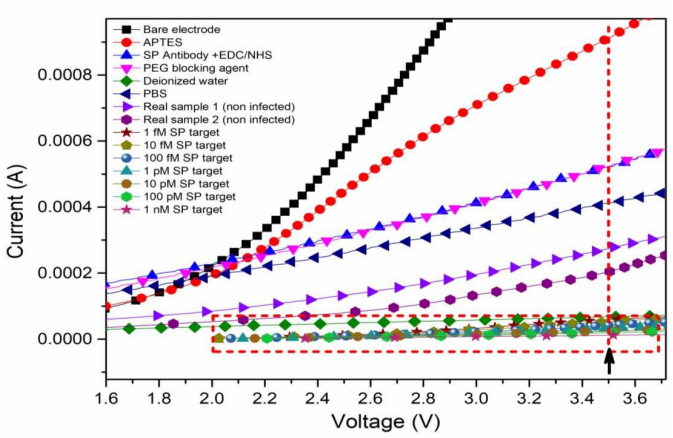

Figure 6. I–V curve of the ARHC-SPE after APTES/antibody/PEG modification and during detection of various samples and COVID-19 target analytes at different concentrations.

From Figure 6, the working function voltage of the ARHC-SPE is identified at 3.5 V. At this voltage, samples showing a current above 0.000065 A are classified as non-complementary targets (negative results), while those below 0.000065 A are considered positive. The graphs highlighted in the red box represent SP target samples at different concentrations, with a clearer view provided with the enlarged image in Figure 7. From this figure, the current decreases as the target concentration increases. This trend indicates an increase in surface resistance due to the binding of complementary SP targets to the immobilized antibodies. According to Ohm's law, where voltage equals current multiplied by resistance, current is inversely proportional to resistance. Therefore, as resistance increases with greater SP target binding, the measured current correspondingly decreases. The use of SP-specific antibodies ensures selective binding of COVID-19 SP targets. In contrast, non-target samples exhibit higher current values (above 0.000065 A), indicating lower resistance and absence of specific binding.

Figure 7 also includes a response from deionized water, which shows low current due to its high resistance and lack of ions. This serves as a baseline reference for determining positive detection. At 3.5 V, increasing SP target concentrations consistently result in decreasing current values. This confirms that the SPE biosensor caneffectively detect COVID-19 SP targets. The sensor shows high sensitivity, with a detection limit to 1 femtomolar (fM), demonstrating its effectiveness for low-concentration detection. The results in Figure 8 indicate that using ARHC/chitosan SPE for COVID-19 testing at 3.5 V shows a positive infection result when the measured current is below 0.0003 A, whereas with bare SPE, a positive result is indicated at currents below 0.00006 A. This shows that the ARHC/chitosan SPE has higher conductivity than the bare SPE. First, with bare SPE, a current measurement below 0.00006 A indicates a positive infection result. This suggests that the electrical conductivity of the bare SPE is relatively low, requiring a very small current to yield a positive test result, indicating higher electrical resistance in the system.

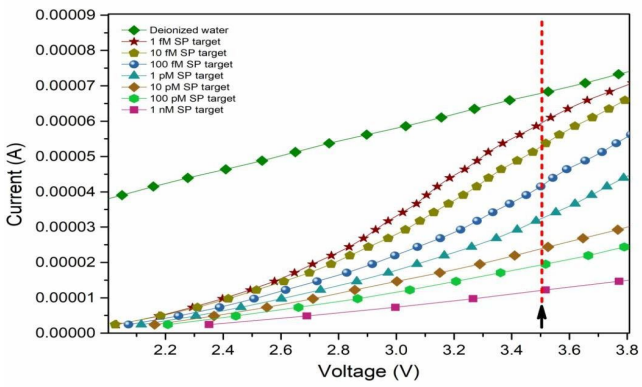

Figure 7. Enlarged image of I-V curve of ARHC-SPE while detecting the COVID-19 target analyte at varying concentrations ranging from 1 fM to 1 nM.

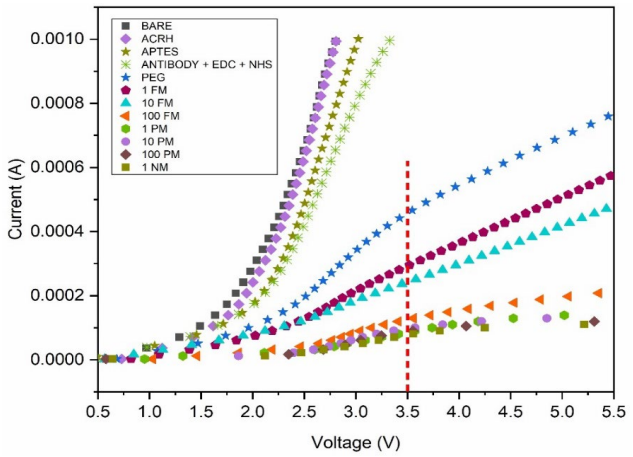

Figure 8. I–V curve of the ARHC/chitosan SPE after APTES/antibody/PEG modification and during detection of various samples and COVID-19 target analytes at different concentrations.

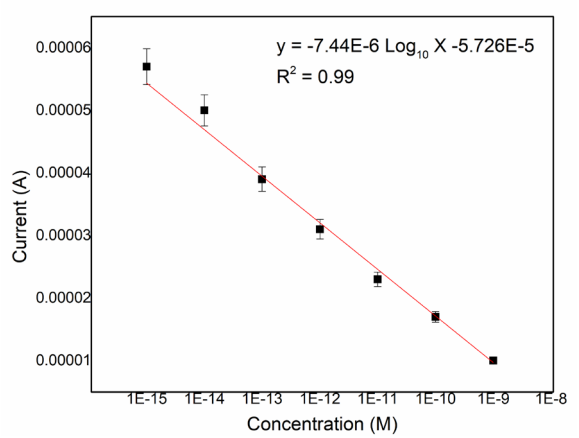

Figure 9. Linear regression analysis of the bare SPE for COVID-19 detection at different concentrations.

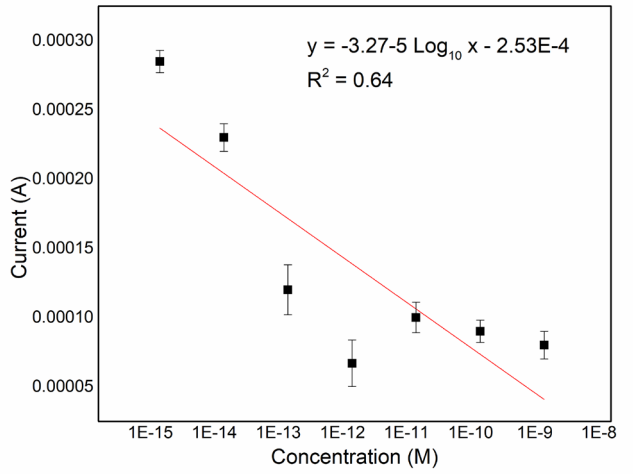

Figure 10. Linear regression analysis of the ARHC/chitosan SPE for COVID-19 detection at different concentrations.

In contrast, using ARHC/chitosan SPE, the threshold for a positive infection result is a measured current below 0.0003 A. This higher current threshold indicates that ARHC/chitosan SPE has lower electrical resistance and thus higher conductivity compared to bare SPE. The lower resistance allows a higher current to flow even at the same applied voltage of 3.5 V, indicating a more sensitive and responsive electrode system for detecting COVID-19 biomarkers. Therefore, the comparison shows that ARHC/chitosan SPE provides higher conductivity than bare SPE under the same experimental conditions. This higher conductivity can improve the performance of ARHC/chitosan SPE, making ital promising candidate for COVID-19 detection assays.

Meanwhile, from the linear regression analysis, both bare SPE and ARHC/chitosan SPE show that the limit of detection for these sensors showed a linear response from 10^{-9} M to

10^{-15} M with an estimated detection capability in the femtomolar range. Although several data points deviated slightly from the fitted regression line for ARHC/chitosan SPE, as can be seen in Figure 10, the deviation remained within acceptable experimental error for electrochemical biosensor measurements at a very low concentration range. This is because such variations are frequently reported in biosensors operating at very low concentrations, such as the femtomolar range, due to increased susceptibility to environmental noise and electrode surface heterogeneity. The overall trend of regression line for ARHC/chitosan still showed a consistent concentration-dependent response, confirming the reliability of the sensing platform.

4. CONCLUSION

In this research, ARHC was prepared by activating rice husk at high temperature, and then characterized for use as a sensitive working electrode for biosensing [10, 11, 14]. Structural and morphological analysis using SEM showed that a porous and rough surface could be formed by the activation, which overcame the surface block of the bare rice husk and offered a more effective surface for adsorption. Functional groups such as –COOH were identified by FTIR spectra, which could anchor the bio-species and enhance the interaction between the electrode and the target. The structure of the prepared material based on the amorphous and porous carbon with several small crystalline peaks working well in the probe [21], an activation-desorption process was monitored by BET experiments. The porosity variations were considerable, contributing to a wide distribution of the surface area ranging from 3.55 m^2/g for bare rice husk up to 242 m^2/g for ARHC and a transition from microporosity to mesoporosity, which would improve the transport properties for mass transfer in a biosensing system. These structural and surface parameters suggested that ARHC could be used as a platform for biosensors. In the I-V measurement, the results show that the conductivity of the SPE has improved with the application of ARHC/chitosan to the SPE working electrode. Future work will focus on optimizing the ARHC synthesis parameters and impedance profile evaluation as well as device integration to validate the ARHC performance in existing practical biosensing applications.

ACKNOWLEDGMENTS

The author gratefully acknowledges support from the Fundamental Research Grant Scheme (FRGS) under grant FRGS/1/2023/STG05/UNIMAP/02/9 from the Ministry of Higher Education, Malaysia.

REFERENCES

[1] Abrego-Martinez J.C., *et al.,* "Nanoscale electrode-aptamer SARS-CoV-2 imaging and electrochemical aptasensors on screen-printed electrodes," *Biosensors & Bioelectronics*, vol. 195, p. 113595, 2022, doi.org/10.1016/j.bios.2021.113595.

[2] Ahmed F., *et al.,* " Fabrication of high-performance asymmetric supercapacitors using rice husk-activated carbon and $MnFe_2O_4$ nanostructures.," *Nanomaterials,* 13, no. 12, p. 1870, 2023, doi.org/10.3390/nano13121870.

[3] Kabay G., *et.al.,* "Emerging biosensing technologies for the diagnostics of viral infectious diseases." *Advanced Materials,* vol. 34, no. 30, p. 2201085, 2022, doi.org/10.1002/adma.202201085.

[4] Antiochia R., "Electrochemical biosensors for SARS-CoV-2 detection: Voltametric or impedimetric transduction?." *Bioelectrochemistry*, vol. 147, p. 108190, 2022, doi.org/10.1016/j.bioelechem.2022.108190.

[5] Mei Y., *et al.,* "Recent progresses in electrochemical DNA biosensors for SARS-CoV-2 detection.", *Frontiers in Bioengineering and Biotechnology*, vol. 10, p. 952510, 2022, doi.org/10.3389/fbioe.2022.952510.

[6] Rubio-Monterde, Ana, Daniel Quesada-Gonzalez, and Arben Merkoci. "Toward integrated molecular lateral flow diagnostic tests using advanced micro-and nanotechnology." *Analytical chemistry*, vol. 95, no. 1, p. 468-489, 2022, doi.org/10.1021/acs.analchem.2c04529.

[7] Cancelliere R., Cianciaruso M., Carbone K., Micheli L., "Biochar: a sustainable alternative in the development of electrochemical printed platforms." *Chemosensors*, 10, no. 8, p. 344, 2022) doi.org/10.3390/chemosensors10080344.

[8] Nandi R., *et al.,* "Impact of KOH activation on rice husk derived porous activated carbon for carbon capture at flue gas alike temperatures with high CO_2/N_2 selectivity." *ACS Omega*, vil. 8, no. 5, p. 4802-4812, 2023, doi.org/10.1021/acsomega.2c06955.

[9] Silva L.R.G., *et al.,* "Electrochemical biosensor for SARS-CoV-2 cDNA detection using AuPs-modified 3D-printed graphene electrodes," *Biosensors*, vol. 12, no. 8, p. 622, 2022, doi.org/10.3390/bios12080622.

[10] Ameku W.A., *et al.,* "Rapid detection of anti-SARS-CoV-2 antibodies with a screen-printed electrode modified with a spike glycoprotein epitope." *Biosensors,* 12, no. 5, p. 272, 2022, doi.org/10.3390/bios12050272.

[11] Barakat N.A.M., *et al.,* "H_3PO_4/KOH activation agent for high performance rice husk activated carbon electrode in acidic media supercapacitors." *Molecules*, 28, no. 1, p. 296 (2022), doi.org/10.3390/molecules28010296.

[12] Qin, Zhiqin, Yuanyuan Ye, Die Zhang, Jiangling He, Jiaojiao Zhou, and Jie Cai. "One/two-step contribution to prepare hierarchical porous carbon derived from rice husk for supercapacitor electrode materials." *ACS omega*, vol. 8, no. 5, p. 5088-5096, 2023, doi.org/10.1021/acsomega.2c07932.

[13] Barakat, Nasser AM, Mohamed S. Mahmoud, and Hager M. Moustafa. "Comparing specific capacitance in rice husk-derived activated carbon through phosphoric acid and potassium hydroxide activation order variations." *Scientific Reports* , vol. 14, no. 1, p. 1460, 2024, doi.org/10.1038/s41598-023-49675-0.

[14] Yerdauletov, M.S., *et. al.,* "Characterization of activated carbon from rice husk for enhanced energy storage devices." *Molecules*, vol 28, no. 15, p. 5818. 2023. doi.org/10.3390/molecules28155818.

[15] Heidarinejad, Zoha, et. al., "Methods for preparation and activation of activated carbon: a review." *Environmental Chemistry Letters,* vol. 18, no. 2, p. 393-415, 2020, doi.org/10.1007/s10311-019-00955-0.

[16] Shahidah et. al., "Comparative analysis of the efficacy of bulk and membrane nanoporous materials in biological sensing" *International Journal of Nanoelectronics and Materials (IJNeaM),* Vol. 18, No. 2, p. 305-313, 2024, doi.org/10.58915/ijneam.v18i2.2188.